

$P_c(4312)^+$, $P_c(4380)^+$, and $P_c(4457)^+$ as novel kinematical effect

Satoshi X. Nakamura^{1,2,*}

¹University of Science and Technology of China, Hefei 230026, People's Republic of China

²State Key Laboratory of Particle Detection and Electronics (IHEP-USTC), Hefei 230036, People's Republic of China

Understanding the nature of the hidden charm pentaquark(like) signals in the LHCb data for $\Lambda_b^0 \rightarrow J/\psi p K^-$ is a central problem of hadron spectroscopy. We propose a scenario completely different from previous ones such as hadron molecules and compact pentaquarks. We identify relevant double triangle mechanisms that cause double triangle singularities. This novel kinematical effect significantly enhances $\Sigma_c^{(*)} \bar{D}^{(*)}$ threshold cusps. Then we demonstrate that the double triangle amplitudes reproduce the peak structures of $P_c(4312)^+$, $P_c(4380)^+$, and $P_c(4457)^+$ in the LHCb data, through an interference with other common mechanisms. Only the $P_c(4440)^+$ peak is due to a resonance with width and strength significantly smaller than previously estimated. P_c signals are expected in other processes and the proposed model (partly) explains the current data such as: the GlueX J/ψ photoproduction data with no P_c signals; the LHCb $\Lambda_b^0 \rightarrow J/\psi p \pi^-$ data with a possible signal only from $P_c(4440)^+$.

Hadron spectrum is a reflection of nonperturbative aspects of QCD. Exotic hadrons have structures different from the conventional quark-antiquark and three-quark [1], and are expected to provide a clue to assess a different aspect of QCD. It is therefore exciting to hear recent experimental discoveries of exotic hadron(like) signals [2–9].

The LHCb Collaboration recently observed in $\Lambda_b^0 \rightarrow J/\psi p K^-$ three resonance(like) structures [10], interpreted as pentaquark states called $P_c(4312)^+$, $P_c(4440)^+$, and $P_c(4457)^+$, by updating their previous analysis [11] that claimed two pentaquarks. Understanding the nature of the P_c 's is certainly a central problem of the hadron spectroscopy. Because of the proximity of the P_c masses to the $\Sigma_c(2455) \bar{D}^{(*)}$ thresholds¹, P_c 's as $\Sigma_c(2455) \bar{D}^{(*)}$ molecules (bound states) may seem a natural interpretation of their identity [13–36]. Yet, constituent pentaquark pictures [37–44] and a hadrocharmonium [45] are also possible options. The LHCb data of the $J/\psi p$ invariant mass ($M_{J/\psi p}$) distribution has been analyzed with a K -matrix model that claimed a virtual state for $P_c(4312)^+$ [46]. Another analyses [34–36] based on one-pion-exchange plus contact interactions for the coupled $\Sigma_c^{(*)} \bar{D}^{(*)}$ system interpreted all the P_c 's as $\Sigma_c^{(*)} \bar{D}^{(*)}$ bound states; they also claimed the existence of $P_c(4380)^+$. So far, all the models assigned a pole to each of the P_c peaks².

In order to establish P_c 's as hadronic states, it is important to confirm their signals in other processes such as

J/ψ photoproduction off a nucleon [48–54]. The GlueX Collaboration conducted such an experiment, finding no evidence [55]. This may indicate that the P_c states couple weakly with a photon, and could be seen in higher statistics data. Another possibility is that the P_c peaks in $\Lambda_b^0 \rightarrow J/\psi p K^-$ are caused by kinematical effects such as threshold cusp and triangle singularity (TS) [56], and do not appear in the photoproduction; however, no relevant mechanism has been found.

In this work, we point out that a double triangle (DT) diagram [Fig. 1(a)] creates a kinematical effect that has not been explored before. The effect is caused by the fact that each loop hits a TS (double TS) in the zero-width limit of unstable particles, and that the two TS can even occur almost simultaneously (quasi-simultaneous double TS). We show that this kinematical effect makes the $\Sigma_c^{(*)} \bar{D}^{(*)}$ threshold cusp significantly more singular. Then we demonstrate that the DT amplitudes reproduce the peak structures of $P_c(4312)^+$, $P_c(4380)^+$, and $P_c(4457)^+$ in the LHCb data, through an interference with other common mechanisms [Figs. 1(b) and 1(d)]. The LHCb data requires this proposed model to have only $P_c(4440)^+$ as a resonance with width and strength significantly smaller than previously estimated. The model can also (partly) explain P_c signals in other data such as: no P_c signals in the J/ψ photoproduction; $\Lambda_b^0 \rightarrow J/\psi p \pi^-$ data [57] suggesting only a $P_c(4440)^+$ signal. In this way, we bring a completely different understanding of the P_c structures of the LHCb data.

Our model for $\Lambda_b^0 \rightarrow J/\psi p K^-$ [Fig. 1] is now discussed. Here we present amplitude formulas for representative cases; see the Supplemental material for complete formulas. We consider parity-conserving mechanisms in partial waves specified by the spin-parity (J^P) of $J/\psi p$; $J^P = 1/2^-, 3/2^-, 1/2^+,$ and $3/2^+$. Although parity-violating mechanisms should also exist, they are redundant in fitting the $M_{J/\psi p}$ distribution data because the kinematical effects are similar for both parities. In what follows, we use the particle mass and width values from Ref. [12], and

¹ We follow the hadron naming scheme of Ref. [12]. For simplicity, however, we often denote $\Sigma_c(2455)^{+(++)}$, $\Sigma_c(2520)^{+(++)}$, $\Lambda_c(2595)^+$, $\Lambda_c(2625)^+$, and J/ψ by Σ_c , Σ_c^* , Λ_c^* , Λ_c^{**} , and ψ , respectively. $\Lambda_c^{(**)}$ and $\Sigma_c^{(*)}$ are also collectively denoted by Y_c . Charge indices are often suppressed.

² Although Ref. [47] claimed $P_c(4457)^+$ to be a threshold cusp, we put the conclusion on hold because: they neither include the $\Sigma_c(2520) \bar{D}$ channel nor fit the structure around its threshold; their fit somewhat missed the $P_c(4312)^+$ peak position.

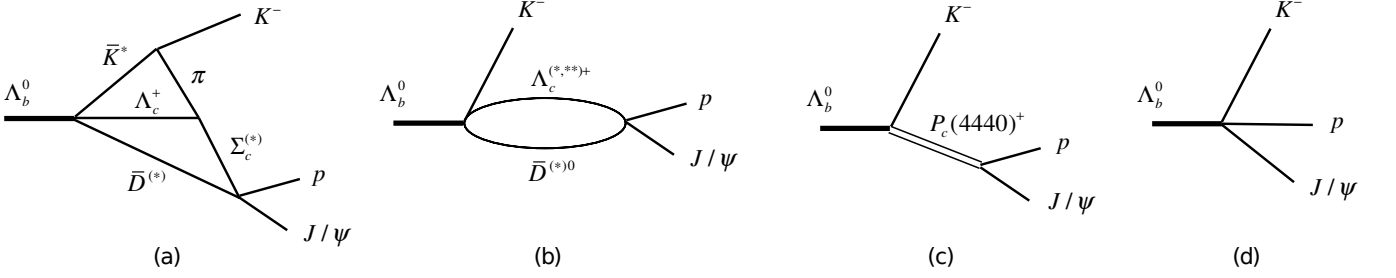


FIG. 1. $\Lambda_b^0 \rightarrow J/\psi p K^-$ decay mechanisms considered in this work: (a) double triangle; (b) one-loop; (c) $P_c(4440)^+$ -excitation; (d) direct decay.

denote the energy, width, momentum, and polarization vector of a particle x by E_x , Γ_x , \mathbf{p}_x , and $\boldsymbol{\epsilon}_x$, respectively. We also denote a meson(M)-baryon(B) pair by $BM(J^P)$. A DT diagram [Fig. 1(a)] that includes $\Sigma_c \bar{D}(1/2^-)$ consists of four vertices such as $\Lambda_b^0 \rightarrow \Lambda_c^+ \bar{D} \bar{K}^*$, $\bar{K}^* \rightarrow \bar{K} \pi$, $\Lambda_c^+ \pi \rightarrow \Sigma_c$, and $\Sigma_c \bar{D}(1/2^-) \rightarrow J/\psi p$ as given by

$$c_{\Lambda_c \bar{D} \bar{K}^*, \Lambda_b} \left(\frac{1}{2} t_{\bar{D}} \frac{1}{2} t_{\bar{K}^*} \middle| 00 \right) \boldsymbol{\sigma} \cdot \boldsymbol{\epsilon}_{\bar{K}^*} F_{\bar{K}^* \bar{D} \Lambda_c, \Lambda_b}^{00}, \quad (1)$$

$$c_{\bar{K} \pi, \bar{K}^*} \left(1 t_{\pi} \frac{1}{2} t_{\bar{K}} \middle| \frac{1}{2} t_{\bar{K}^*} \right) \boldsymbol{\epsilon}_{\bar{K}^*} \cdot (\mathbf{p}_{\bar{K}} - \mathbf{p}_{\pi}) f_{\bar{K} \pi, \bar{K}^*}^1, \quad (2)$$

$$c_{\Lambda_c \pi, \Sigma_c} \boldsymbol{\sigma} \cdot \mathbf{p}_{\pi} f_{\Lambda_c \pi, \Sigma_c}^1, \quad (3)$$

$$c_{\psi p, \Sigma_c \bar{D}}^{1/2^-} \left(1 t_{\Sigma_c} \frac{1}{2} t_{\bar{D}} \middle| \frac{1}{2} t_p \right) \boldsymbol{\sigma} \cdot \boldsymbol{\epsilon}_{\psi} f_{\psi p}^0 f_{\Sigma_c \bar{D}}^0, \quad (4)$$

respectively. Dipole form factors with a cutoff Λ are denoted by $F_{ijk,l}^{LL'}$, f_{ij}^L , and $f_{ij,k}^L$. The parentheses are isospin Clebsch-Gordan coefficients (CGCs) with t_x being the isospin z -component of x . In Eq. (1) and later in Eq. (6), we assume that color-favored Λ_b^0 decays dominate over color-suppressed ones, and thus the isospin of the $\bar{D}^{(*)} \bar{K}^{(*)}$ pair is 0³. The couplings $c_{\bar{K} \pi, \bar{K}^*}$ and $c_{\Lambda_c \pi, \Sigma_c}$ are determined using the K^* and $\Sigma_c(2455)$ decay widths. The DT amplitude is

$$\begin{aligned} A_{\Sigma_c \bar{D}(1/2^-)}^{\text{DT}} &= \sum_{\text{charge}} c_{\psi p, \Sigma_c \bar{D}}^{1/2^-} c_{\Lambda_c \pi, \Sigma_c} c_{\bar{K} \pi, \bar{K}^*} c_{\Lambda_c \bar{D} \bar{K}^*, \Lambda_b} \\ &\times (\text{isospin CGCs}) \int d^3 p_{\pi} \int d^3 p_{\bar{D}} \\ &\times \frac{\boldsymbol{\sigma} \cdot \boldsymbol{\epsilon}_{\psi} \boldsymbol{\sigma} \cdot \mathbf{p}_{\pi}}{E - E_{\bar{K}} - E_{\Sigma_c} - E_{\bar{D}} + \frac{i}{2} \Gamma_{\Sigma_c}} \\ &\times \frac{\boldsymbol{\sigma} \cdot (\mathbf{p}_{\bar{K}} - \mathbf{p}_{\pi})}{E - E_{\bar{K}} - E_{\pi} - E_{\Lambda_c} - E_{\bar{D}} + i\epsilon} \\ &\times \frac{f_{\psi p}^0 f_{\Sigma_c \bar{D}}^0 f_{\Lambda_c \pi, \Sigma_c}^1 f_{\bar{K} \pi, \bar{K}^*}^1 F_{\bar{K}^* \bar{D} \Lambda_c, \Lambda_b}^{00}}{E - E_{\bar{K}^*} - E_{\Lambda_c} - E_{\bar{D}} + \frac{i}{2} \Gamma_{K^*}}, \quad (5) \end{aligned}$$

³ Our model does not include color-suppressed $\Lambda_b^0 \rightarrow \Sigma_c^{(*)} \bar{D}^{(*)} K^-$ vertices, used in hadron molecule models, that might cause a problem in explaining P_c production rates [26].

where different charge states in the loops are summed with charge dependent particle masses. The amplitude is implicitly sandwiched by initial Λ_b^0 and final p spin state.

The $\Lambda_c^+ \bar{D}^{*0}(1/2^-)$ one-loop amplitude [Fig. 1(b)] is composed by an initial $\Lambda_b^0 \rightarrow \Lambda_c^+ \bar{D}^{*0} K^-$ decay vertex

$$c_{\Lambda_c \bar{D}^* \bar{K}, \Lambda_b} \left(\frac{1}{2} t_{\bar{D}^*} \frac{1}{2} t_{\bar{K}} \middle| 00 \right) \boldsymbol{\sigma} \cdot \boldsymbol{\epsilon}_{\bar{D}^*} F_{\bar{K} \bar{D}^* \Lambda_c, \Lambda_b}^{00}, \quad (6)$$

and the subsequent $\Lambda_c^+ \bar{D}^{*0}(1/2^-) \rightarrow J/\psi p$ interaction

$$c_{\psi p, \Lambda_c \bar{D}^*}^{1/2^-} \boldsymbol{\sigma} \cdot \boldsymbol{\epsilon}_{\psi} \boldsymbol{\sigma} \cdot \boldsymbol{\epsilon}_{\bar{D}^*} f_{\psi p}^0 f_{\Lambda_c \bar{D}^*}^0. \quad (7)$$

Thus the one-loop amplitude is

$$\begin{aligned} A_{\Lambda_c \bar{D}^*}^{1\text{L}} &= 3 c_{\psi p, \Lambda_c \bar{D}^*}^{1/2^-} c_{\Lambda_c \bar{D}^* \bar{K}, \Lambda_b} \left(\frac{1}{2} t_{\bar{D}^*} \frac{1}{2} t_{\bar{K}} \middle| 00 \right) \boldsymbol{\sigma} \cdot \boldsymbol{\epsilon}_{\psi} \\ &\times \int d^3 p_{\bar{D}^*} \frac{f_{\psi p}^0 f_{\Lambda_c \bar{D}^*}^0 F_{\bar{K} \bar{D}^* \Lambda_c, \Lambda_b}^{00}}{E - E_{\bar{K}} - E_{\Lambda_c} - E_{\bar{D}^*} + \frac{i}{2} \Gamma_{D^*}}, \quad (8) \end{aligned}$$

with $\Gamma_{D^{*0}} = 55$ keV [58].

The $P_c(4440)^+$ amplitude [Fig. 1(c)] is given in the Breit-Wigner form with adjustable $P_c(4440)^+$ mass, width, and coupling. As J^P of $P_c(4440)^+$, we examine $1/2^{\pm}$ and $3/2^{\pm}$ cases. The internal structure of $P_c(4440)^+$ is beyond the scope of this work. We also consider a direct decay mechanism [Fig. 1(d)] in each partial wave with a real coupling strength. This simulates all mechanisms that do not belong to the diagrams of Figs. 1(a)-1(c).

The $Y_c \bar{D}^{(*)}$ pairs in the DT and one-loop diagrams require a nonperturbative treatment. Meanwhile, the lattice QCD [59] found that the $J/\psi p \rightarrow J/\psi p$ interaction is very weak. Thus we use a single-channel contact interaction model [60] to calculate a $Y_c \bar{D}^{(*)}$ scattering amplitude that maintains only the elastic unitarity. Then, a perturbative transition to $J/\psi p$ follows. The resulting $Y_c \bar{D}^{(*)} \rightarrow J/\psi p$ amplitude is implemented in Eqs. (5) and (8); see the Supplemental material. Other possible coupled-channel effects are assumed to be absorbed by complex couplings fitted to the data.

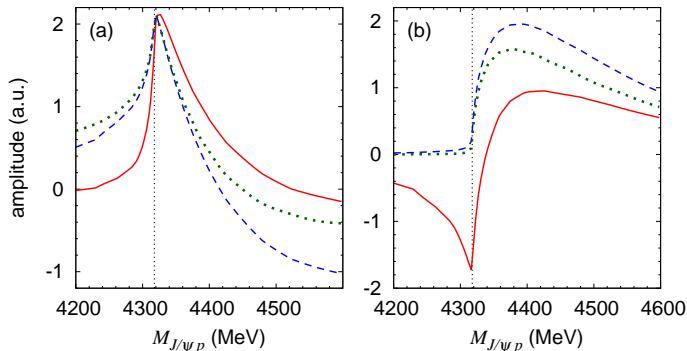


FIG. 2. Double triangle amplitude of Fig. 1(a) for $\Sigma_c^{(*)} \bar{D}^{(*)} = \Sigma_c^+ \bar{D}^0$; $\Lambda = 1$ GeV; $\Sigma_c^+ \bar{D}^0 \rightarrow J/\psi p$ is treated perturbatively. The panel (a) [(b)] shows the real [imaginary] part of the amplitudes. The red solid curves are for the double triangle diagram, and they reduce to the blue dashed ones by using $m_{\Lambda_c^+} = 3$ GeV. The green dotted curves are a $\Sigma_c^+ \bar{D}^0$ one-loop amplitude. All the amplitudes are normalized so that the real parts have the same peak height. The dotted vertical lines indicate the $\Sigma_c^+ \bar{D}^0$ threshold.

As mentioned earlier, the DT amplitudes cause double TS and some of them even hit quasi-simultaneous double TS. Just like the common TS from a single triangle diagram [56], the quasi-simultaneous double TS occurs in a special condition where the DT process is kinematically allowed at the classical level. Details on the kinematical conditions and concrete examples for the quasi-simultaneous double TS are given in the Supplemental material. We note that, while the common TS directly enhances the amplitude, the double TS contribution to the DT amplitudes is more indirect. This is because the double TS appears in a small part of the whole space spanned by the loop momenta and, after the loop integral, its effect is largely hidden in other contributions. Yet, the double TS may give a visible effect.

We plot in Fig. 2 the DT amplitude that includes $\Sigma_c^+ \bar{D}^0(1/2^-)$ [red solid curves]. A singular behavior clearly shows up at the $\Sigma_c^+ \bar{D}^0$ threshold. For comparison, we plot a typical threshold cusp behavior from a one-loop amplitude of Fig. 1(b) in which $\Lambda_c^+ \bar{D}^{*0}$ is replaced by $\Sigma_c^+ \bar{D}^0$ [green dotted curves]. The DT amplitude is clearly more singular due to the double TS. For an illustration, we replace the Λ_c^+ mass in the DT amplitude with a hypothetically heavy value (3 GeV) so that the loop integral does not hit the double TS. The resultant amplitude [blue dashed curves] now behaves like an ordinary threshold cusp. We note that the amplitudes shown in Fig. 2 include $\Sigma_c^+ \bar{D}^0 \rightarrow J/\psi p$ treated as the first-order perturbation. If this process is described non-perturbatively with an attractive $\Sigma_c^+ \bar{D}^0$ interaction, the singular behaviors in Fig. 2 become even sharper [61].

As expected from Fig. 2, the DT amplitude alone creates a peak at the $\Sigma_c^{(*)} \bar{D}^{(*)}$ threshold in the $M_{J/\psi p}$ dis-

tribution of $\Lambda_b^0 \rightarrow J/\psi p K^-$. This peak cannot be identified with the P_c^+ peak which is located slightly below the threshold. However, suppose there exists a flat amplitude that destructively (constructively) interferes with the real (imaginary) part of the DT amplitude of Fig. 2. This coherent sum would generate a peak slightly below the $\Sigma_c^{(*)} \bar{D}^{(*)}$ threshold. This is how the P_c^+ -like structures (other than $P_c(4440)^+$) show up from the DT mechanisms.

For describing $\Lambda_b^0 \rightarrow J/\psi p K^-$, our full model includes: (i) DT mechanisms with $\Sigma_c(2455) \bar{D}(1/2^-)$, $\Sigma_c(2520) \bar{D}(3/2^-)$, $\Sigma_c(2455) \bar{D}^*(1/2^-)$, $\Sigma_c(2455) \bar{D}^*(3/2^-)$, $\Sigma_c(2520) \bar{D}^*(1/2^-)$, and $\Sigma_c(2520) \bar{D}^*(3/2^-)$; (ii) one-loop mechanisms with $\Lambda_c^+ \bar{D}^{*0}(1/2^-)$, $\Lambda_c(2595)^+ \bar{D}^0(1/2^+)$, and $\Lambda_c(2625)^+ \bar{D}^0(3/2^+)$; (iii) $P_c(4440)^+$ mechanism; (iv) direct decay mechanisms. Regarding the number of fitting parameters, each mechanism in the items (i)-(iii) has an adjustable complex overall factor to fit the data; 2×10 parameters. Each direct decay mechanism (iv) has a real coupling strength; 4 parameters. The $P_c(4440)^+$ mass and width are adjustable. We also adjust a repulsive $\Lambda_c^+ \bar{D}^{*0}$ interaction strength. Because the overall absolute normalization of the full amplitude is arbitrary, we have totally 26 parameters.

Regarding the $Y_c \bar{D}^{(*)}$ interaction strengths, we examine if the fit favors an attractive or repulsive interaction for a given $BM(J^P)$. The fit favors attractions for $\Sigma_c(2455) \bar{D}(1/2^-)$, $\Sigma_c(2520) \bar{D}(3/2^-)$, $\Sigma_c(2455) \bar{D}^*(1/2^-)$, $\Sigma_c(2455) \bar{D}^*(3/2^-)$, $\Lambda_c(2595)^+ \bar{D}^0(1/2^+)$, $\Lambda_c(2625)^+ \bar{D}^0(3/2^+)$, and repulsions for $\Sigma_c(2520) \bar{D}^*(1/2^-)$, $\Sigma_c(2520) \bar{D}^*(3/2^-)$, $\Lambda_c^+ \bar{D}^{*0}(1/2^-)$. Then we fix the coupling strength so that the scattering length is $a \sim 0.5$ fm⁴ for the attraction. The repulsive $\Lambda_c^+ \bar{D}^{*0}(1/2^-)$ interaction strength is fitted to the data because the fit quality is rather sensitive; $a \sim -0.4, -0.2$, and -0.05 fm for $\Lambda \sim 800, 1000$, and 1500 – 2000 MeV, respectively. The other repulsive interactions use the same strength as $\Lambda_c^+ \bar{D}^{*0}$. It is noted that, within our model, spectrum peak positions are not very sensitive to a values. The cutoff in the form factors is fixed at $\Lambda = 1$ GeV unless otherwise stated. Only the direct decay amplitudes include different cutoffs on $p_{\bar{K}}$ so that their $M_{J/\psi p}$ distribution is similar to the phase-space shape.

We compare in Fig. 3(a) our calculation with the LHCb data [10]. The experimental resolution is considered in the calculation. Our full model (red solid curve) well fits the data. The $P_c(4312)^+$, $P_c(4380)^+$, and $P_c(4457)^+$ peaks are well described by the kinematical effects from the considered mechanisms, and not by poles near the peak positions. Only the $P_c(4440)^+$ peak requires a resonance pole for which we choose $J^P = 3/2^-$ in the figure.

⁴ The scattering length (a) is related to the phase shift (δ) by $p \cot \delta = 1/a + \mathcal{O}(p^2)$.

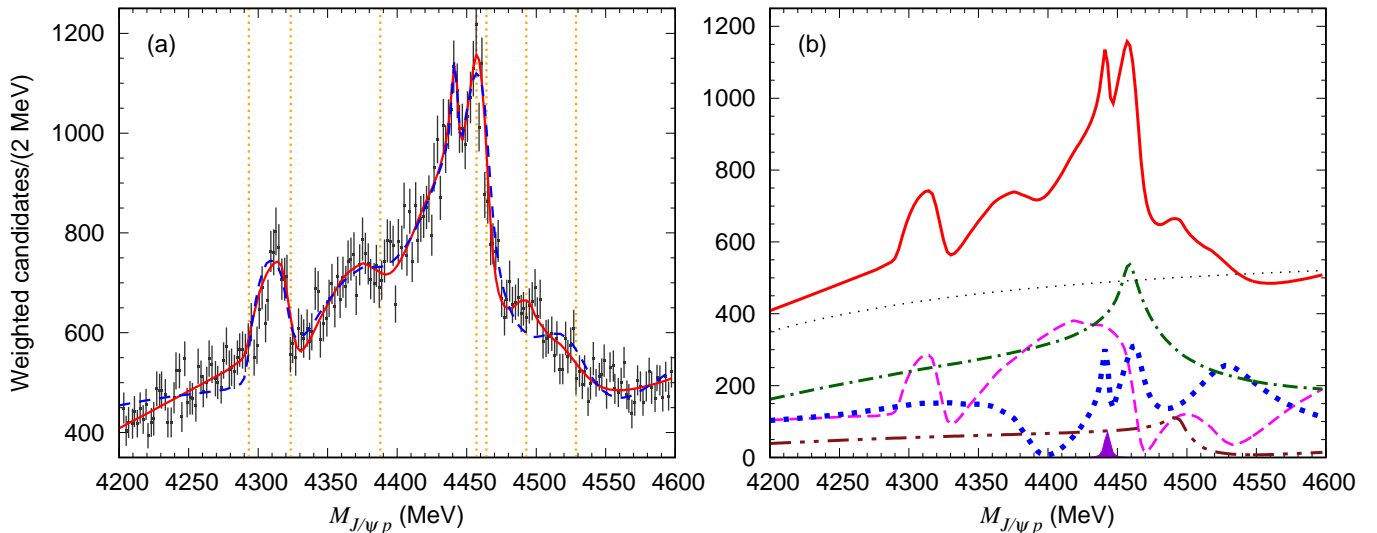


FIG. 3. $J/\psi p$ invariant mass ($M_{J/\psi p}$) distribution for $\Lambda_b^0 \rightarrow J/\psi p K^-$. (a) Comparison with the LHCb data ($\cos\theta_{P_c}$ -weighted samples) [10]. The red solid (blue dashed) curve is from the full (simplified) model; see the text for details on the models. The dotted vertical lines indicate the threshold energies for, from left to right, $\Lambda_c^+ \bar{D}^{*0}$, $\Sigma_c(2455)^{++} D^-$, $\Sigma_c(2520)^{++} D^-$, $\Lambda_c(2595)^+ \bar{D}^0$, $\Sigma_c(2455)^{++} D^{*-}$, $\Lambda_c(2625)^+ \bar{D}^0$, and $\Sigma_c(2520)^{++} D^{*-}$, respectively. (b) Partial wave contributions specified by J^P of the $J/\psi p$ pair. The magenta dashed, blue dotted, green dash-dotted, and brown dash-two-dotted curves are for $J^P = 1/2^-, 3/2^-, 1/2^+$, and $3/2^+$, respectively. The solid violet peak is the $P_c(4440)^+(3/2^-)$ contribution without interference. The thin black dotted curve is the sum of direct decay mechanisms. The red solid curve is from the full model.

The fit quality does not significantly change when varying the cutoff over $\Lambda = 0.8$ –2 GeV and when choosing $J^P = 1/2^\pm$ and $3/2^\pm$ for $P_c(4440)^+$; the fits thus do not favor a particular J^P of $P_c(4440)^+$. We now simplify the model by omitting the $1/2^+$ and $3/2^+$ amplitudes, and treating $Y_c \bar{D}^{(*)} \rightarrow J/\psi p$ perturbatively. With 19 parameters to refit, the main features of the data are fairly well captured (blue dashed curve). Still, the structures are less sharp near the thresholds because of lacking the strong $Y_c \bar{D}^{(*)}$ scattering. The $1/2^+$ and $3/2^+$ amplitudes are also needed for a more precise fit.

In Fig. 3(b), we show the full model’s partial wave contributions that do not interfere with each other in the $M_{J/\psi p}$ distribution. In the $1/2^-$ (magenta dashed curve) and $3/2^-$ (blue dotted curve) contributions, as discussed earlier, the interference between the DT and direct decay mechanisms creates bumps slightly below the $\Sigma_c^{(*)} \bar{D}^{(*)}$ thresholds where the peaks of $P_c(4312)^+$, $P_c(4380)^+$, and $P_c(4457)^+$ are located. The $1/2^-$ contribution also shows a bent due to the $\Lambda_c^+ \bar{D}^{*0}$ threshold cusp, being consistent with the LHCb data. The $1/2^+$ (green dash-dotted curve) and $3/2^+$ (brown dash-two-dotted curve) contributions exhibit $\Lambda_c(2595)^+ \bar{D}^0$ and $\Lambda_c(2625)^+ \bar{D}^0$ threshold cusps, respectively, capturing the characteristic structures in the data. Although the $1/2^+$ peak seems a large contribution, this is due to a constructive interference between the $\Lambda_c(2595)^+ \bar{D}^0$ one-loop and direct decay amplitudes; the $\Lambda_c(2595)^+ \bar{D}^0$ one-loop amplitude itself is significantly smaller than the $\Lambda_c^+ \bar{D}^{*0}$ one-loop amplitude

in magnitude. The sum of the direct decay mechanisms shows a phase-space-like distribution (thin black dotted curve). We note that this partial wave decomposition would involve an uncertainty due to the limited experimental information.

The $P_c(4440)^+(3/2^-)$ contribution without interference is shown by the violet solid peak in Fig. 3(b). The $P_c(4440)^+(3/2^-)$ mass and width from our fit is 4443.3 ± 1.4 MeV and 2.7 ± 2.2 MeV, respectively⁵. The cutoff dependence is safely within the errors. Comparing with the LHCb analysis [10], $4440.3 \pm 1.3_{-4.7}^{+4.1}$ MeV and $20.6 \pm 4.9_{-10.1}^{+8.7}$ MeV, the width is significantly narrower. Also, the $P_c(4440)^+$ contribution is only $\sim 1/22$ of the LHCb’s estimate: $\mathcal{R} \equiv \mathcal{B}(\Lambda_b^0 \rightarrow P_c^+ K^-) \mathcal{B}(P_c^+ \rightarrow J/\psi p) / \mathcal{B}(\Lambda_b^0 \rightarrow J/\psi p K^-) = 1.11 \pm 0.33_{-0.10}^{+0.22}$ %. This difference arises because the LHCb fitted the structure at $M_{J/\psi p} \sim 4450$ MeV with the incoherent $P_c(4440)^+$ and $P_c(4457)^+$ contributions while we describe a large body of the structure with the kinematical effects and only the small spike is attributed to the $P_c(4440)^+$ and its interference.

The quality of the fit could be slightly improved with more attractive $\Sigma_c^{(*)} \bar{D}^{(*)}$ interactions. However, such interactions generate virtual poles near the thresholds and,

⁵ The statistical errors on the $P_c(4440)^+$ parameters are estimated just for a reference by varying only the $P_c(4440)^+$ mass, width, and coupling.

as a result, $\gamma p \rightarrow J/\psi p$ cross section would have sharp peaks at the $\Sigma_c^{(*)} \bar{D}^{(*)}$ thresholds. Since the GlueX did not find such peaks [55], we fix the $\Sigma_c^{(*)} \bar{D}^{(*)}$ interactions at the modest strength so that no poles are generated close to the thresholds⁶.

One may wonder if the magnitude of the DT amplitudes would be significantly suppressed compared to other mechanisms. This question may be addressed by comparing the coupling strength of the DT amplitude [Eq. (5)] and that of the $\Lambda_c^+ \bar{D}^{*0}$ one-loop amplitude [Eq. (8)]. We introduce a ratio by

$$R = \frac{\left| \frac{c_{\psi p, \Sigma_c \bar{D}}^{1/2^-} c_{\Lambda_c \bar{D} \bar{K}^*, \Lambda_b}}{c_{\psi p, \Lambda_c \bar{D}^*}^{1/2^-} c_{\Lambda_c \bar{D}^* \bar{K}, \Lambda_b}} \right|}{}, \quad (9)$$

where well-controlled parameters ($c_{\bar{K}\pi, \bar{K}^*}$, etc.) are not included. Fitting the LHCb data gives $R = 3.6 - 1.6$ for $\Lambda = 0.8 - 2$ GeV. Thus, unnaturally large parameter values ($R \gg 1$) are not necessary, indicating that the comparable strengths of the DT and one-loop amplitudes are not an artifact.

Our model partly explains the absence of P_c^+ signals in J/ψ photoproduction data [55]. All P_c^+ peaks, except for $P_c(4440)^+$, in $\Lambda_b^0 \rightarrow J/\psi p K^-$ are caused by the kinematical effect (DT mechanisms and its interference) that requires an accompanying K^- in the final state. The $\gamma p \rightarrow J/\psi p$ process cannot accommodate this kinematical effect and, thus, has no P_c^+ signals. For $P_c(4440)^+$, its width and fit fraction from our analysis are significantly smaller than those extracted in the LHCb's analysis. In this case, observing a $P_c(4440)^+$ signal in J/ψ photoproduction would be more challenging than expected based on the LHCb result.

An evidence for P_c was also found in $\Lambda_b^0 \rightarrow J/\psi p \pi^-$ [57]. The $M_{J/\psi p}$ distribution [Fig. 3(b) of [57]] seems to indicate that the $M_{J/\psi p}$ bin of $P_c(4440)^+$ has an enhancement, whereas this is not the case for the other P_c 's. This observation is consistent with what our model implies: the $P_c(4440)^+$ [DT] mechanisms in $\Lambda_b^0 \rightarrow J/\psi p K^-$ can [cannot] be shared by $\Lambda_b^0 \rightarrow J/\psi p \pi^-$, and thus only $P_c(4440)^+$ appears in the latter. Since the current data is statistically limited, P_c signals in $\Lambda_b^0 \rightarrow J/\psi p \pi^-$ are still inconclusive. Higher statistics data is eagerly awaited.

An interesting next step would be to apply our model to $\Lambda_b^0 \rightarrow \Sigma_c^{(*)} \bar{D}^{(*)} K^-$. Our model has, as a main mechanism, the diagram of Fig. 1(a) with the last $\Sigma_c^{(*)} \bar{D}^{(*)} \rightarrow J/\psi p$ vertex removed (single triangle diagram). An immediate prediction from this mechanism is TS peaks at $M_{\Sigma_c K^-} \sim 3.40$ GeV and $M_{\Sigma_c^* K^-} \sim 3.21$ GeV. Searching for and understanding other resonancelike structures with the double TS is also an interesting direction.

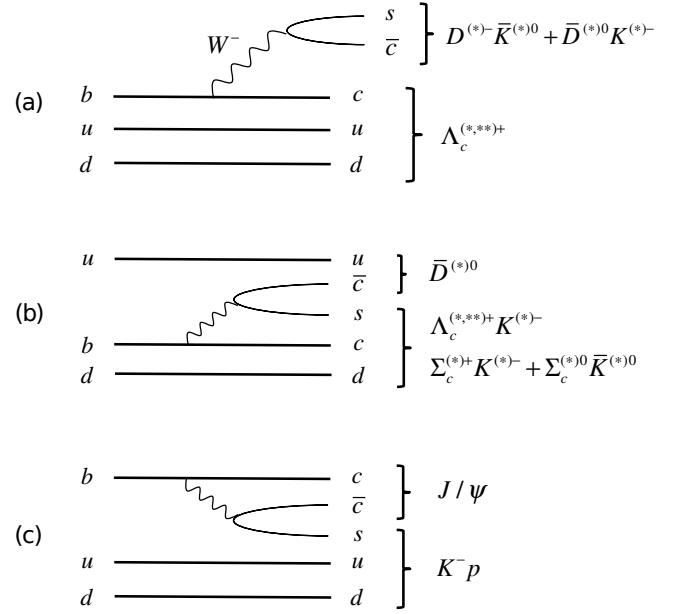


FIG. 4. Quark diagrams for Λ_b^0 decay vertices. (a) Color-favored diagram; (b,c) Color-suppressed diagrams.

This work is in part supported by National Natural Science Foundation of China (NSFC) under contracts U2032103 and 11625523, and also by National Key Research and Development Program of China under Contracts Nos. 2020YFA0406400.

Supplemental material

1. $\Lambda_b^0 \rightarrow J/\psi p K^-$ amplitudes

We present formulas for diagrams of Fig. 1. For the present study, we consider only parity-conserving mechanisms. For double triangle (DT) diagrams of Fig. 1(a), we consider those including $\Sigma_c \bar{D}(1/2^-)$, $\Sigma_c^* \bar{D}(3/2^-)$, $\Sigma_c \bar{D}^*(1/2^-)$, $\Sigma_c \bar{D}^*(3/2^-)$, $\Sigma_c^* \bar{D}^*(1/2^-)$, and $\Sigma_c^* \bar{D}^*(3/2^-)$ pairs going to $J/\psi p$ [$\Sigma_c \equiv \Sigma_c(2455)^{+,++}$, $\Sigma_c^* \equiv \Sigma_c(2520)^{+,++}$]. Each of the DT diagrams includes four vertices. The initial one is either $\Lambda_b^0 \rightarrow \Lambda_c^+ \bar{D} \bar{K}^*$ or $\Lambda_b^0 \rightarrow \Lambda_c^+ \bar{D}^* \bar{K}^*$ vertices given by

$$c_{\Lambda_c \bar{D} \bar{K}^*, \Lambda_b} \left(\frac{1}{2} t_{\bar{D}} \frac{1}{2} t_{\bar{K}^*} \middle| 00 \right) \sigma \cdot \epsilon_{\bar{K}^*} F_{\bar{K}^* \bar{D} \Lambda_c, \Lambda_b}^{00}, \quad (10)$$

$$c_{\Lambda_c \bar{D}^* \bar{K}^*, \Lambda_b} \left(\frac{1}{2} t_{\bar{D}^*} \frac{1}{2} t_{\bar{K}^*} \middle| 00 \right) i \sigma \cdot (\epsilon_{\bar{K}^*} \times \epsilon_{\bar{D}^*}) F_{\bar{K}^* \bar{D}^* \Lambda_c, \Lambda_b}^{00}, \quad (11)$$

respectively, where the coupling constants $c_{\Lambda_c \bar{D} \bar{K}^*, \Lambda_b}$ and $c_{\Lambda_c \bar{D}^* \bar{K}^*, \Lambda_b}$ are generally complex values. Here and later in Eqs. (29)-(31), we assume that color-favored Λ_b^0 decays [Fig. 4(a)] dominate over color-suppressed ones [Fig. 4(b)], and thus the isospin of the $\bar{D}^{(*)} \bar{K}^{(*)}$ pair is

⁶ Our $\Sigma_c \bar{D}$ interaction model with $a \sim 0.5$ fm generates a virtual pole at ~ 20 MeV below the threshold.

0. We have used dipole form factors $F_{ijk,l}^{LL'}$ given as

$$F_{ijk,l}^{LL'} = \frac{1}{\sqrt{E_i E_j E_k E_l}} \left(\frac{\Lambda^2}{\Lambda^2 + q_{ij}^2} \right)^{2+\frac{l}{2}} \left(\frac{\Lambda'^2}{\Lambda'^2 + \tilde{p}_k^2} \right)^{2+\frac{l'}{2}} \quad (12)$$

where q_{ij} (\tilde{p}_k) is the momentum of i (k) in the ij (total) center-of-mass frame. The second vertex, $\bar{K}^* \rightarrow \bar{K}\pi$ is common for all the DT diagram, and is given as

$$c_{\bar{K}\pi, \bar{K}^*} \left(1t_\pi \frac{1}{2} t_{\bar{K}} \left| \frac{1}{2} t_{\bar{K}^*} \right. \right) \epsilon_{\bar{K}^*} \cdot (\mathbf{p}_{\bar{K}} - \mathbf{p}_\pi) f_{\bar{K}\pi, \bar{K}^*}^1 \quad (13)$$

with the form factor $f_{ij,k}^L \equiv f_{ij}^L / \sqrt{E_k}$ and

$$f_{ij}^L = \frac{1}{\sqrt{E_i E_j}} \left(\frac{\Lambda^2}{\Lambda^2 + q_{ij}^2} \right)^{2+(L/2)}. \quad (14)$$

The third vertex is either $\Lambda_c \pi \rightarrow \Sigma_c$ or $\Lambda_c \pi \rightarrow \Sigma_c^*$ which are given by

$$c_{\Lambda_c \pi, \Sigma_c} \boldsymbol{\sigma} \cdot \mathbf{p}_\pi f_{\Lambda_c \pi, \Sigma_c}^1, \quad (15)$$

$$c_{\Lambda_c \pi, \Sigma_c^*} \mathbf{S}^\dagger \cdot \mathbf{p}_\pi f_{\Lambda_c \pi, \Sigma_c^*}^1, \quad (16)$$

respectively. We have introduced baryon spin operators \mathbf{S}^\dagger and \mathbf{S} that change a baryon spin as $\frac{1}{2} \rightarrow \frac{3}{2}$ and $\frac{3}{2} \rightarrow \frac{1}{2}$, respectively; they can be expressed with the Pauli matrices as $\mathbf{S} \cdot \mathbf{a} \mathbf{S}^\dagger \cdot \mathbf{b} = \frac{2}{3} \mathbf{a} \cdot \mathbf{b} - \frac{i}{3} \boldsymbol{\sigma} \cdot (\mathbf{a} \times \mathbf{b})$. The

fourth vertices cause transitions $\Sigma_c \bar{D}(1/2^-)$, $\Sigma_c^* \bar{D}(3/2^-)$, $\Sigma_c \bar{D}^*(1/2^-)$, $\Sigma_c \bar{D}^*(3/2^-)$, $\Sigma_c^* \bar{D}^*(1/2^-)$, $\Sigma_c^* \bar{D}^*(3/2^-) \rightarrow J/\psi p$ as given by

$$c_{\psi p, \Sigma_c \bar{D}}^{1/2^-} \left(1t_{\Sigma_c} \frac{1}{2} t_{\bar{D}} \left| \frac{1}{2} t_p \right. \right) \boldsymbol{\sigma} \cdot \boldsymbol{\epsilon}_\psi f_{\psi p}^0 f_{\Sigma_c \bar{D}}^0, \quad (17)$$

$$c_{\psi p, \Sigma_c^* \bar{D}}^{3/2^-} \left(1t_{\Sigma_c^*} \frac{1}{2} t_{\bar{D}} \left| \frac{1}{2} t_p \right. \right) \mathbf{S} \cdot \boldsymbol{\epsilon}_\psi f_{\psi p}^0 f_{\Sigma_c^* \bar{D}}^0, \quad (18)$$

$$c_{\psi p, \Sigma_c \bar{D}^*}^{1/2^-} \left(1t_{\Sigma_c} \frac{1}{2} t_{\bar{D}^*} \left| \frac{1}{2} t_p \right. \right) \boldsymbol{\sigma} \cdot \boldsymbol{\epsilon}_\psi \boldsymbol{\sigma} \cdot \boldsymbol{\epsilon}_{\bar{D}^*} f_{\psi p}^0 f_{\Sigma_c \bar{D}^*}^0, \quad (19)$$

$$c_{\psi p, \Sigma_c \bar{D}^*}^{3/2^-} \left(1t_{\Sigma_c} \frac{1}{2} t_{\bar{D}^*} \left| \frac{1}{2} t_p \right. \right) \mathbf{S} \cdot \boldsymbol{\epsilon}_\psi \mathbf{S}^\dagger \cdot \boldsymbol{\epsilon}_{\bar{D}^*} f_{\psi p}^0 f_{\Sigma_c \bar{D}^*}^0, \quad (20)$$

$$c_{\psi p, \Sigma_c^* \bar{D}^*}^{1/2^-} \left(1t_{\Sigma_c^*} \frac{1}{2} t_{\bar{D}^*} \left| \frac{1}{2} t_p \right. \right) \boldsymbol{\sigma} \cdot \boldsymbol{\epsilon}_\psi \mathbf{S} \cdot \boldsymbol{\epsilon}_{\bar{D}^*} f_{\psi p}^0 f_{\Sigma_c^* \bar{D}^*}^0, \quad (21)$$

$$c_{\psi p, \Sigma_c^* \bar{D}^*}^{3/2^-} \left(1t_{\Sigma_c^*} \frac{1}{2} t_{\bar{D}^*} \left| \frac{1}{2} t_p \right. \right) \mathbf{S} \cdot \boldsymbol{\epsilon}_\psi \mathbf{S}_{\frac{3}{2}} \cdot \boldsymbol{\epsilon}_{\bar{D}^*} f_{\psi p}^0 f_{\Sigma_c^* \bar{D}^*}^0, \quad (22)$$

respectively; $\mathbf{S}_{\frac{3}{2}}$ is a spin operator defined with Clebsch-Gordan coefficient as $\langle m' | S_{\frac{3}{2}}^k | m \rangle \equiv \left(\frac{3}{2} m 1 k \left| \frac{3}{2} m' \right. \right)$ where $|m^{(\prime)}\rangle$ is a spin state of a spin-3/2 particle. The DT amplitudes including $\Sigma_c^{(*)} \bar{D}^{(*)}(J^P)$, denoted by $A_{\Sigma_c^{(*)} \bar{D}^{(*)}(J^P)}^{\text{DT}}$, are constructed with the above ingredients as

$$A_{\Sigma_c \bar{D}(1/2^-)}^{\text{DT}} = c_{\psi p, \Sigma_c \bar{D}}^{1/2^-} c_{\Lambda_c \pi, \Sigma_c} c_{\bar{K}\pi, \bar{K}^*} c_{\Lambda_c \bar{D} \bar{K}^*, \Lambda_b} \left(1t_{\Sigma_c} \frac{1}{2} t_{\bar{D}} \left| \frac{1}{2} t_p \right. \right) \left(1t_\pi \frac{1}{2} t_{\bar{K}} \left| \frac{1}{2} t_{\bar{K}^*} \right. \right) \left(\frac{1}{2} t_{\bar{D}} \frac{1}{2} t_{\bar{K}^*} \left| 00 \right. \right) \int d^3 p_\pi \int d^3 p_{\bar{D}} \\ \times \frac{\boldsymbol{\sigma} \cdot \boldsymbol{\epsilon}_\psi \boldsymbol{\sigma} \cdot \mathbf{p}_\pi}{E - E_{\bar{K}} - E_{\Sigma_c} - E_{\bar{D}} + \frac{i}{2} \Gamma_{\Sigma_c}} \frac{\boldsymbol{\sigma} \cdot (\mathbf{p}_{\bar{K}} - \mathbf{p}_\pi)}{E - E_{\bar{K}} - E_\pi - E_{\Lambda_c} - E_{\bar{D}} + i\epsilon} \frac{f_{\psi p}^0 f_{\Sigma_c \bar{D}}^0 f_{\Lambda_c \pi, \Sigma_c}^1 f_{\bar{K}\pi, \bar{K}^*}^1 f_{\bar{K}^* \bar{D} \Lambda_c, \Lambda_b}^0}{E - E_{\bar{K}^*} - E_{\Lambda_c} - E_{\bar{D}} + \frac{i}{2} \Gamma_{K^*}}, \quad (23)$$

$$A_{\Sigma_c^* \bar{D}(3/2^-)}^{\text{DT}} = c_{\psi p, \Sigma_c^* \bar{D}}^{3/2^-} c_{\Lambda_c \pi, \Sigma_c^*} c_{\bar{K}\pi, \bar{K}^*} c_{\Lambda_c \bar{D} \bar{K}^*, \Lambda_b} \left(1t_{\Sigma_c^*} \frac{1}{2} t_{\bar{D}} \left| \frac{1}{2} t_p \right. \right) \left(1t_\pi \frac{1}{2} t_{\bar{K}} \left| \frac{1}{2} t_{\bar{K}^*} \right. \right) \left(\frac{1}{2} t_{\bar{D}} \frac{1}{2} t_{\bar{K}^*} \left| 00 \right. \right) \int d^3 p_\pi \int d^3 p_{\bar{D}} \\ \times \frac{\mathbf{S} \cdot \boldsymbol{\epsilon}_\psi \mathbf{S}^\dagger \cdot \mathbf{p}_\pi}{E - E_{\bar{K}} - E_{\Sigma_c^*} - E_{\bar{D}} + \frac{i}{2} \Gamma_{\Sigma_c^*}} \frac{\boldsymbol{\sigma} \cdot (\mathbf{p}_{\bar{K}} - \mathbf{p}_\pi)}{E - E_{\bar{K}} - E_\pi - E_{\Lambda_c} - E_{\bar{D}} + i\epsilon} \frac{f_{\psi p}^0 f_{\Sigma_c^* \bar{D}}^0 f_{\Lambda_c \pi, \Sigma_c^*}^1 f_{\bar{K}\pi, \bar{K}^*}^1 f_{\bar{K}^* \bar{D} \Lambda_c, \Lambda_b}^0}{E - E_{\bar{K}^*} - E_{\Lambda_c} - E_{\bar{D}} + \frac{i}{2} \Gamma_{K^*}}, \quad (24)$$

$$A_{\Sigma_c \bar{D}^*(1/2^-)}^{\text{DT}} = c_{\psi p, \Sigma_c \bar{D}^*}^{1/2^-} c_{\Lambda_c \pi, \Sigma_c} c_{\bar{K}\pi, \bar{K}^*} c_{\Lambda_c \bar{D}^* \bar{K}^*, \Lambda_b} \left(1t_{\Sigma_c} \frac{1}{2} t_{\bar{D}^*} \left| \frac{1}{2} t_p \right. \right) \left(1t_\pi \frac{1}{2} t_{\bar{K}} \left| \frac{1}{2} t_{\bar{K}^*} \right. \right) \left(\frac{1}{2} t_{\bar{D}^*} \frac{1}{2} t_{\bar{K}^*} \left| 00 \right. \right) \int d^3 p_\pi \int d^3 p_{\bar{D}^*} \\ \times \frac{\sum_{\epsilon_{\bar{D}^*}} \boldsymbol{\sigma} \cdot \boldsymbol{\epsilon}_\psi \boldsymbol{\sigma} \cdot \boldsymbol{\epsilon}_{\bar{D}^*} \boldsymbol{\sigma} \cdot \mathbf{p}_\pi}{E - E_{\bar{K}} - E_{\Sigma_c} - E_{\bar{D}^*} + \frac{i}{2} \Gamma_{\Sigma_c}} \frac{i \boldsymbol{\sigma} \cdot [(\mathbf{p}_{\bar{K}} - \mathbf{p}_\pi) \times \boldsymbol{\epsilon}_{\bar{D}^*}]}{E - E_{\bar{K}} - E_\pi - E_{\Lambda_c} - E_{\bar{D}^*} + i\epsilon} \frac{f_{\psi p}^0 f_{\Sigma_c \bar{D}^*}^0 f_{\Lambda_c \pi, \Sigma_c}^1 f_{\bar{K}\pi, \bar{K}^*}^1 f_{\bar{K}^* \bar{D}^* \Lambda_c, \Lambda_b}^0}{E - E_{\bar{K}^*} - E_{\Lambda_c} - E_{\bar{D}^*} + \frac{i}{2} \Gamma_{K^*}}, \quad (25)$$

$$A_{\Sigma_c \bar{D}^*(3/2^-)}^{\text{DT}} = c_{\psi p, \Sigma_c \bar{D}^*}^{3/2^-} c_{\Lambda_c \pi, \Sigma_c} c_{\bar{K}\pi, \bar{K}^*} c_{\Lambda_c \bar{D}^* \bar{K}^*, \Lambda_b} \left(1t_{\Sigma_c} \frac{1}{2} t_{\bar{D}^*} \left| \frac{1}{2} t_p \right. \right) \left(1t_\pi \frac{1}{2} t_{\bar{K}} \left| \frac{1}{2} t_{\bar{K}^*} \right. \right) \left(\frac{1}{2} t_{\bar{D}^*} \frac{1}{2} t_{\bar{K}^*} \left| 00 \right. \right) \int d^3 p_\pi \int d^3 p_{\bar{D}^*} \\ \times \frac{\sum_{\epsilon_{\bar{D}^*}} \mathbf{S} \cdot \boldsymbol{\epsilon}_\psi \mathbf{S}^\dagger \cdot \boldsymbol{\epsilon}_{\bar{D}^*} \boldsymbol{\sigma} \cdot \mathbf{p}_\pi}{E - E_{\bar{K}} - E_{\Sigma_c} - E_{\bar{D}^*} + \frac{i}{2} \Gamma_{\Sigma_c}} \frac{i \boldsymbol{\sigma} \cdot [(\mathbf{p}_{\bar{K}} - \mathbf{p}_\pi) \times \boldsymbol{\epsilon}_{\bar{D}^*}]}{E - E_{\bar{K}} - E_\pi - E_{\Lambda_c} - E_{\bar{D}^*} + i\epsilon} \frac{f_{\psi p}^0 f_{\Sigma_c \bar{D}^*}^0 f_{\Lambda_c \pi, \Sigma_c}^1 f_{\bar{K}\pi, \bar{K}^*}^1 f_{\bar{K}^* \bar{D}^* \Lambda_c, \Lambda_b}^0}{E - E_{\bar{K}^*} - E_{\Lambda_c} - E_{\bar{D}^*} + \frac{i}{2} \Gamma_{K^*}}, \quad (26)$$

$$\begin{aligned}
A_{\Sigma_c^* \bar{D}^* (1/2^-)}^{\text{DT}} &= c_{\psi p, \Sigma_c^* \bar{D}^*}^{1/2^-} c_{\Lambda_c \pi, \Sigma_c^*} c_{\bar{K} \pi, \bar{K}^*} c_{\Lambda_c \bar{D}^* \bar{K}^*, \Lambda_b} \left(1 t_{\Sigma_c^*} \frac{1}{2} t_{\bar{D}^*} \left| \frac{1}{2} t_p \right. \right) \left(1 t_{\pi} \frac{1}{2} t_{\bar{K}} \left| \frac{1}{2} t_{\bar{K}^*} \right. \right) \left(\frac{1}{2} t_{\bar{D}^*} \frac{1}{2} t_{\bar{K}^*} \left| 00 \right. \right) \int d^3 p_{\pi} \int d^3 p_{\bar{D}^*} \\
&\times \frac{\sum_{\epsilon_{\bar{D}^*}} \boldsymbol{\sigma} \cdot \boldsymbol{\epsilon}_{\psi} \mathbf{S} \cdot \boldsymbol{\epsilon}_{\bar{D}^*} \mathbf{S}^{\dagger} \cdot \mathbf{p}_{\pi}}{E - E_{\bar{K}} - E_{\Sigma_c^*} - E_{\bar{D}^*} + \frac{i}{2} \Gamma_{\Sigma_c^*}} \frac{i \boldsymbol{\sigma} \cdot [(\mathbf{p}_{\bar{K}} - \mathbf{p}_{\pi}) \times \boldsymbol{\epsilon}_{\bar{D}^*}]}{E - E_{\bar{K}} - E_{\pi} - E_{\Lambda_c} - E_{\bar{D}^*} + i\epsilon} \frac{f_{\psi p}^0 f_{\Sigma_c^* \bar{D}^*}^0 f_{\Lambda_c \pi, \Sigma_c^*}^1 f_{\bar{K} \pi, \bar{K}^*}^1 F_{\bar{K}^* \bar{D}^* \Lambda_c, \Lambda_b}^{00}}{E - E_{\bar{K}^*} - E_{\Lambda_c} - E_{\bar{D}^*} + \frac{i}{2} \Gamma_{K^*}}, \quad (27)
\end{aligned}$$

$$\begin{aligned}
A_{\Sigma_c^* \bar{D}^* (3/2^-)}^{\text{DT}} &= c_{\psi p, \Sigma_c^* \bar{D}^*}^{3/2^-} c_{\Lambda_c \pi, \Sigma_c^*} c_{\bar{K} \pi, \bar{K}^*} c_{\Lambda_c \bar{D}^* \bar{K}^*, \Lambda_b} \left(1 t_{\Sigma_c^*} \frac{1}{2} t_{\bar{D}^*} \left| \frac{1}{2} t_p \right. \right) \left(1 t_{\pi} \frac{1}{2} t_{\bar{K}} \left| \frac{1}{2} t_{\bar{K}^*} \right. \right) \left(\frac{1}{2} t_{\bar{D}^*} \frac{1}{2} t_{\bar{K}^*} \left| 00 \right. \right) \int d^3 p_{\pi} \int d^3 p_{\bar{D}^*} \\
&\times \frac{\sum_{\epsilon_{\bar{D}^*}} \mathbf{S} \cdot \boldsymbol{\epsilon}_{\psi} \mathbf{S}_{3/2} \cdot \boldsymbol{\epsilon}_{\bar{D}^*} \mathbf{S}^{\dagger} \cdot \mathbf{p}_{\pi}}{E - E_{\bar{K}} - E_{\Sigma_c^*} - E_{\bar{D}^*} + \frac{i}{2} \Gamma_{\Sigma_c^*}} \frac{i \boldsymbol{\sigma} \cdot [(\mathbf{p}_{\bar{K}} - \mathbf{p}_{\pi}) \times \boldsymbol{\epsilon}_{\bar{D}^*}]}{E - E_{\bar{K}} - E_{\pi} - E_{\Lambda_c} - E_{\bar{D}^*} + i\epsilon} \frac{f_{\psi p}^0 f_{\Sigma_c^* \bar{D}^*}^0 f_{\Lambda_c \pi, \Sigma_c^*}^1 f_{\bar{K} \pi, \bar{K}^*}^1 F_{\bar{K}^* \bar{D}^* \Lambda_c, \Lambda_b}^{00}}{E - E_{\bar{K}^*} - E_{\Lambda_c} - E_{\bar{D}^*} + \frac{i}{2} \Gamma_{K^*}}, \quad (28)
\end{aligned}$$

where, in each amplitude, the summation over the two charged states with the charge dependent particle masses is implicit; the tiny Γ_{D^*} has been neglected. It is understood that the amplitudes are implicitly sandwiched by initial Λ_b^0 and final p spin state.

Next we present formulas for the one-loop diagrams of Fig. 1(b) including the $\Lambda_c^+ \bar{D}^{*0} (1/2^-)$, $\Lambda_c (2593)^+ \bar{D}^0 (1/2^+)$, and $\Lambda_c (2625)^+ \bar{D}^0 (3/2^+)$ loops. The initial decay vertices are:

$$c_{\Lambda_c \bar{D}^* \bar{K}, \Lambda_b} \left(\frac{1}{2} t_{\bar{D}^*} \frac{1}{2} t_{\bar{K}} \left| 00 \right. \right) \boldsymbol{\sigma} \cdot \boldsymbol{\epsilon}_{\bar{D}^*} F_{\bar{K} \bar{D}^* \Lambda_c, \Lambda_b}^{00}, \quad (29)$$

$$c_{\Lambda_c^* \bar{D} \bar{K}, \Lambda_b} \left(\frac{1}{2} t_{\bar{D}} \frac{1}{2} t_{\bar{K}} \left| 00 \right. \right) \boldsymbol{\sigma} \cdot (\mathbf{p}_{\bar{K}} - \mathbf{p}_{\bar{D}}) F_{\bar{K} \bar{D} \Lambda_c^*, \Lambda_b}^{10}, \quad (30)$$

$$c_{\Lambda_c^{**} \bar{D} \bar{K}, \Lambda_b} \left(\frac{1}{2} t_{\bar{D}} \frac{1}{2} t_{\bar{K}} \left| 00 \right. \right) \mathbf{S}^{\dagger} \cdot (\mathbf{p}_{\bar{K}} - \mathbf{p}_{\bar{D}}) F_{\bar{K} \bar{D} \Lambda_c^{**}, \Lambda_b}^{10}, \quad (31)$$

for $\Lambda_b^0 \rightarrow \Lambda_c^+ \bar{D}^{*0} K^-, \Lambda_c^{*+} \bar{D}^0 K^-,$ and $\Lambda_c^{**+} \bar{D}^0 K^-,$ respectively [$\Lambda_c^* \equiv \Lambda_c(2595)^+, \Lambda_c^{**} \equiv \Lambda_c(2625)^+$]. The coupling constants $c_{\Lambda_c^{(*,**) \bar{D}^*} \bar{K}, \Lambda_b}$ are generally complex values. The subsequent interactions for $\Lambda_c^+ \bar{D}^{*0} (1/2^-), \Lambda_c^{*+} \bar{D}^0 (1/2^+), \Lambda_c^{**+} \bar{D}^0 (3/2^+) \rightarrow J/\psi p$ are

$$c_{\psi p, \Lambda_c \bar{D}^*}^{1/2^-} \boldsymbol{\sigma} \cdot \boldsymbol{\epsilon}_{\psi} \boldsymbol{\sigma} \cdot \boldsymbol{\epsilon}_{\bar{D}^*} f_{\psi p}^0 f_{\Lambda_c \bar{D}^*}^0, \quad (32)$$

$$c_{\psi p, \Lambda_c^* \bar{D}}^{1/2^+} \boldsymbol{\sigma} \cdot \boldsymbol{\epsilon}_{\psi} \boldsymbol{\sigma} \cdot \mathbf{p}_{\psi} f_{\psi p}^1 f_{\Lambda_c^* \bar{D}}^0, \quad (33)$$

$$c_{\psi p, \Lambda_c^{**} \bar{D}}^{3/2^+} \boldsymbol{\sigma} \cdot \boldsymbol{\epsilon}_{\psi} \mathbf{S} \cdot \mathbf{p}_{\psi} f_{\psi p}^1 f_{\Lambda_c^{**} \bar{D}}^0, \quad (34)$$

respectively. The one-loop amplitudes including $\Lambda_c^{(*,**) \bar{D}^*} (1/2^-)$, denoted by $A_{\Lambda_c^{(*,**) \bar{D}^*}}^{\text{1L}}$, are given with the above ingredients as

$$A_{\Lambda_c \bar{D}^*}^{\text{1L}} = 3 c_{\psi p, \Lambda_c \bar{D}^*}^{1/2^-} c_{\Lambda_c \bar{D}^* \bar{K}, \Lambda_b} \left(\frac{1}{2} t_{\bar{D}^*} \frac{1}{2} t_{\bar{K}} \left| 00 \right. \right) \boldsymbol{\sigma} \cdot \boldsymbol{\epsilon}_{\psi} \int d^3 p_{\bar{D}^*} \frac{f_{\psi p}^0 f_{\Lambda_c \bar{D}^*}^0 F_{\bar{K} \bar{D}^* \Lambda_c, \Lambda_b}^{00}}{E - E_{\bar{K}} - E_{\Lambda_c} - E_{\bar{D}^*} + \frac{i}{2} \Gamma_{D^*}}, \quad (35)$$

$$A_{\Lambda_c^* \bar{D}}^{\text{1L}} = c_{\psi p, \Lambda_c^* \bar{D}}^{1/2^+} c_{\Lambda_c^* \bar{D} \bar{K}, \Lambda_b} \left(\frac{1}{2} t_{\bar{D}} \frac{1}{2} t_{\bar{K}} \left| 00 \right. \right) \boldsymbol{\sigma} \cdot \boldsymbol{\epsilon}_{\psi} \boldsymbol{\sigma} \cdot \mathbf{p}_{\psi} \int d^3 p_{\bar{D}} \boldsymbol{\sigma} \cdot (\mathbf{p}_{\bar{K}} - \mathbf{p}_{\bar{D}}) \frac{f_{\psi p}^1 f_{\Lambda_c^* \bar{D}}^0 F_{\bar{K} \bar{D} \Lambda_c^*, \Lambda_b}^{10}}{E - E_{\bar{K}} - E_{\Lambda_c^*} - E_{\bar{D}} + \frac{i}{2} \Gamma_{\Lambda_c^*}}, \quad (36)$$

$$A_{\Lambda_c^{**} \bar{D}}^{\text{1L}} = c_{\psi p, \Lambda_c^{**} \bar{D}}^{3/2^+} c_{\Lambda_c^{**} \bar{D} \bar{K}, \Lambda_b} \left(\frac{1}{2} t_{\bar{D}} \frac{1}{2} t_{\bar{K}} \left| 00 \right. \right) \boldsymbol{\sigma} \cdot \boldsymbol{\epsilon}_{\psi} \mathbf{S} \cdot \mathbf{p}_{\psi} \int d^3 p_{\bar{D}} \mathbf{S}^{\dagger} \cdot (\mathbf{p}_{\bar{K}} - \mathbf{p}_{\bar{D}}) \frac{f_{\psi p}^1 f_{\Lambda_c^{**} \bar{D}}^0 F_{\bar{K} \bar{D} \Lambda_c^{**}, \Lambda_b}^{10}}{E - E_{\bar{K}} - E_{\Lambda_c^{**}} - E_{\bar{D}} + \frac{i}{2} \Gamma_{\Lambda_c^{**}}}. \quad (37)$$

The resonant $P_c(4440)^+$ amplitude of Fig. 1(c) is given as

$$A_{P_c(4440)}^{1/2^-} = c_{P_c(4440)}^{1/2^-} \frac{\boldsymbol{\sigma} \cdot \boldsymbol{\epsilon}_{\psi} f_{\psi p, P_c}^0 f_{P_c \bar{K}, \Lambda_b}^0}{E - E_{\bar{K}} - E_{P_c} + \frac{i}{2} \Gamma_{P_c}}, \quad (38)$$

for $P_c(4440)^+$ of $J^P = 1/2^-$,

$$\begin{aligned}
A_{P_c(4440)}^{3/2^-} &= c_{P_c(4440)}^{3/2^-} \mathbf{S} \cdot \boldsymbol{\epsilon}_{\psi} \mathbf{S}^{\dagger} \cdot \mathbf{p}_{\bar{K}} \boldsymbol{\sigma} \cdot \mathbf{p}_{\bar{K}} \\
&\times \frac{f_{\psi p, P_c}^0 f_{P_c \bar{K}, \Lambda_b}^2}{E - E_{\bar{K}} - E_{P_c} + \frac{i}{2} \Gamma_{P_c}}, \quad (39)
\end{aligned}$$

for $P_c(4440)^+$ of $J^P = 3/2^-$,

$$\begin{aligned}
A_{P_c(4440)}^{1/2^+} &= c_{P_c(4440)}^{1/2^+} \boldsymbol{\sigma} \cdot \boldsymbol{\epsilon}_{\psi} \boldsymbol{\sigma} \cdot \mathbf{p}_{\psi} \boldsymbol{\sigma} \cdot \mathbf{p}_{\bar{K}} \\
&\times \frac{f_{\psi p, P_c}^1 f_{P_c \bar{K}, \Lambda_b}^1}{E - E_{\bar{K}} - E_{P_c} + \frac{i}{2} \Gamma_{P_c}}, \quad (40)
\end{aligned}$$

for $P_c(4440)^+$ of $J^P = 1/2^+$, and

$$A_{P_c(4440)}^{3/2^+} = c_{P_c(4440)}^{3/2^+} \boldsymbol{\sigma} \cdot \boldsymbol{\epsilon}_\psi \mathbf{S} \cdot \mathbf{p}_\psi \mathbf{S}^\dagger \cdot \mathbf{p}_{\bar{K}} \\ \times \frac{f_{\psi p, P_c}^1 f_{P_c \bar{K}, \Lambda_b}^1}{E - E_{\bar{K}} - E_{P_c} + \frac{i}{2} \Gamma_{P_c}}, \quad (41)$$

for $P_c(4440)^+$ of $J^P = 3/2^+$.

The direct decays [Fig. 1(d)] may mainly originate from a color-suppressed quark diagram of Fig. 4(c). The corresponding amplitudes can be projected onto the $pJ/\psi(J^P)$ partial waves. Thus we employ a form as follows:

$$A_{\text{dir}} = c_{\text{dir}}^{1/2^-} \boldsymbol{\sigma} \cdot \boldsymbol{\epsilon}_\psi F_{\psi p \bar{K}, \Lambda_b}^{00} \\ + c_{\text{dir}}^{3/2^-} \mathbf{S} \cdot \boldsymbol{\epsilon}_\psi \mathbf{S}^\dagger \cdot \mathbf{p}_{\bar{K}} \boldsymbol{\sigma} \cdot \mathbf{p}_{\bar{K}} F_{\psi p \bar{K}, \Lambda_b}^{02} \\ + c_{\text{dir}}^{1/2^+} \boldsymbol{\sigma} \cdot \boldsymbol{\epsilon}_\psi \boldsymbol{\sigma} \cdot \mathbf{p}_\psi \boldsymbol{\sigma} \cdot \mathbf{p}_{\bar{K}} F_{\psi p \bar{K}, \Lambda_b}^{11} \\ + c_{\text{dir}}^{3/2^+} \boldsymbol{\sigma} \cdot \boldsymbol{\epsilon}_\psi \mathbf{S} \cdot \mathbf{p}_\psi \mathbf{S}^\dagger \cdot \mathbf{p}_{\bar{K}} F_{\psi p \bar{K}, \Lambda_b}^{11}, \quad (42)$$

where $c_{\text{dir}}^{J^P}$ is a (real) coupling constant for the $pJ/\psi(J^P)$ partial wave amplitude; the lowest orbital angular momentum between $pJ/\psi(J^P)$ and K^- is considered. We basically use the common cutoff value for all the vertices discussed above. One exception applies to Eq. (42) where we adjust Λ' of Eq. (12) so that the $M_{J/\psi p}$ distribution from the direct decay amplitude is similar to the phase-space shape.

In numerical calculations, for convenience, all the above amplitudes are evaluated in the $J/\psi p$ center-of-mass frame. With the relevant kinematical factors multiplied, the invariant amplitudes are obtained and plugged into the Dalitz plot distribution formula. See Appendix B of Ref. [62] for details.

2. $Y_c \bar{D}^{(*)} \rightarrow J/\psi p$ amplitudes

We describe a single-channel $Y_c \bar{D}^{(*)}$ s -wave scattering (isospin 1/2) with an interaction potential as follows [60]:

$$v_\alpha(q', q) = \left(T_{Y_c} t'_{Y_c} \frac{1}{2} t'_{\bar{D}^{(*)}} \left| \frac{11}{22} \right. \right) \left(T_{Y_c} t_{Y_c} \frac{1}{2} t_{\bar{D}^{(*)}} \left| \frac{11}{22} \right. \right) \\ \times f_\alpha^0(q') h_\alpha f_\alpha^0(q), \quad (43)$$

where a label α specifies one of $Y_c \bar{D}^{(*)}$ and its J^P ; the isospin of Y_c and its z -component are denoted by T_{Y_c} and $t_{Y_c}^{(\prime)}$, respectively. h_α is a coupling constant. The form factor f_α^0 has been defined in Eq. (14). With the above interaction potential, the elastic $Y_c \bar{D}^{(*)}$ scattering amplitude is given as follows:

$$t_\alpha(p', p; E) = \left(T_{Y_c} t'_{Y_c} \frac{1}{2} t'_{\bar{D}^{(*)}} \left| \frac{11}{22} \right. \right) \left(T_{Y_c} t_{Y_c} \frac{1}{2} t_{\bar{D}^{(*)}} \left| \frac{11}{22} \right. \right) \\ \times f_\alpha^0(p') \frac{h_\alpha}{1 - h_\alpha \sigma_\alpha(E)} f_\alpha^0(p), \quad (44)$$

with

$$\sigma_\alpha(E) = \sum_{\text{charge}} \left(T_{Y_c} t_{Y_c} \frac{1}{2} t_{\bar{D}^{(*)}} \left| \frac{11}{22} \right. \right)^2 \\ \times \int dq q^2 \frac{[f_\alpha^0(q)]^2}{E - E_{Y_c}(q) - E_{\bar{D}^{(*)}}(q) + \frac{i}{2} \Gamma_{Y_c}} \quad (45)$$

where the summation runs over $\Sigma_c^{(*)+} \bar{D}^{(*)0}$ and $\Sigma_c^{(*)++} \bar{D}^{(*)-}$ for $Y_c = \Sigma_c^{(*)}$; the mass splitting of the different charge states are taken care of; no summation for $Y_c = \Lambda_c^{(*, **)}$. The tiny Γ_{D^*} has been neglected in Eq. (45). Assuming a perturbative $Y_c \bar{D}^{(*)} \rightarrow J/\psi p$ interaction, we then obtain

$$c_{\psi p, \alpha}^{J^P \alpha} \left(T_{Y_c} t_{Y_c} \frac{1}{2} t_{\bar{D}^{(*)}} \left| \frac{11}{22} \right. \right) f_{\psi p}^0(p') f_\alpha^0(p) [1 - h_\alpha \sigma_\alpha(E)]^{-1}, \quad (46)$$

for the $Y_c \bar{D}^{(*)} \rightarrow J/\psi p$ transition amplitude. Now the DT amplitudes of our full model are obtained by multiplying $[1 - h_\alpha \sigma_\alpha(E)]^{-1}$ with $E = M_{J/\psi p}$ to Eqs. (5) and (23)-(28). The DT amplitudes without this modification are used in the simplified model. Similarly, the one-loop amplitudes of the full model are obtained by multiplying $[1 - h_\alpha \sigma_\alpha(E)]^{-1}$ to Eqs. (8) and (35)-(37). The one-loop amplitudes without this modification are used in the simplified model.

3. Double triangle singularity in double triangle diagram

The loop integral in the DT amplitude [Eqs. (23)-(28)] hits triangle singularities (TS) from upper and lower triangles of Fig. 1(a) (double TS) in the zero-width limit of unstable particles in the loops. Furthermore, the two TS can even occur almost simultaneously (quasi-simultaneous double TS). The conditions for the exactly simultaneous double TS are: (i) $E = E_1 = E_2 = E_3$ (on-shell condition) with $E_1 \equiv E_{\bar{K}^*} + E_{\Lambda_c} + E_{\bar{D}^{(*)}}$, $E_2 \equiv E_{\bar{K}} + E_\pi + E_{\Lambda_c} + E_{\bar{D}^{(*)}}$, and $E_3 \equiv E_{\bar{K}} + E_{\Sigma_c^{(*)}} + E_{\bar{D}^{(*)}}$; (ii) the internal momenta are all collinear in the center-of-mass frame; (iii) classically allowed kinematics [$\hat{p}_{\bar{K}^*} \cdot \hat{p}_\pi = -1$, $\hat{p}_{\bar{D}^{(*)}} \cdot \hat{p}_{\Sigma_c^{(*)}} = 1$, $v_\pi (\equiv |\mathbf{p}_\pi|/E_\pi) \geq v_{\Lambda_c^+}$, $v_{\bar{D}^{(*)}} \geq v_{\Lambda_c^+}$, and $v_{\Sigma_c^{(*)}} \geq v_{\bar{D}^{(*)}}$ for the case of $\hat{p}_{\Lambda_c} \cdot \hat{p}_{\bar{D}^{(*)}} = 1$]. While a simultaneous double TS satisfies all the above conditions, we examine realistic cases where the conditions (ii) and (iii) are satisfied but (i) is partly satisfied: (i') $E = E_1 = E_2 \neq E_3$ [$E = E_2 = E_3 \neq E_1$] for which a TS occurs only in the upper [lower] triangle of Fig. 1(a).

In each of Tables I and II, we present a set of particle momenta (center-of-mass frame) from Eqs. (23)-(28) that satisfies the above conditions (i'), (ii) and (iii). Table I (II) corresponds to the case of $E = E_1 = E_2 \neq E_3$ ($E = E_2 = E_3 \neq E_1$), and $|E_3 - E| \lesssim \Gamma_{K^*}$ ($|E_1 - E| \lesssim \Gamma_{K^*}$) may indicate a quasi-simultaneous double TS. For this calculation, the K^- momentum is set along the positive

axis, and charge dependent masses are averaged. The tables show that the quasi-simultaneous double TS conditions are (not) satisfied by $A_{\Sigma_c \bar{D}}^{\text{DT}}$ and $A_{\Sigma_c \bar{D}^*}^{\text{DT}}$ ($A_{\Sigma_c^* \bar{D}}^{\text{DT}}$ and $A_{\Sigma_c^* \bar{D}^*}^{\text{DT}}$). This fact (and also a smaller effect from $\Gamma_{\Sigma_c} < \Gamma_{\Sigma_c^*}$ [$\Gamma_{\Sigma_c^*} \sim 15$ MeV and $\Gamma_{\Sigma_c} \sim 2$ MeV]) makes $A_{\Sigma_c \bar{D}}^{\text{DT}}$ and $A_{\Sigma_c \bar{D}^*}^{\text{DT}}$ more singular than $A_{\Sigma_c^* \bar{D}}^{\text{DT}}$ and $A_{\Sigma_c^* \bar{D}^*}^{\text{DT}}$ near the $\Sigma_c^{(*)} \bar{D}^{(*)}$ thresholds. This seems consistent with the result in Fig. 3.

* satoshi@ustc.edu.cn

- [1] S. Godfrey and N. Isgur, Mesons in a relativized quark model with chromodynamics, Phys. Rev. D **32**, 189 (1985).
- [2] H.-X. Chen, W. Chen, X. Liu, and S.-L. Zhu, The hidden-charm pentaquark and tetraquark states, Phys. Rep. **639**, 1 (2016).
- [3] A. Hosaka, T. Iijima, K. Miyabayashi, Y. Sakai, and S. Yasui, Exotic hadrons with heavy flavors: X , Y , Z , and related states, PTEP **2016**, 062C01 (2016).
- [4] R.F. Lebed, R.E. Mitchell, and E.S. Swanson, Heavy-Quark QCD Exotica, Prog. Part. Nucl. Phys. **93**, 143 (2017).
- [5] A. Esposito, A. Pilloni, and A.D. Polosa, Multiquark Resonances, Phys. Rept. **668**, 1 (2017).
- [6] A. Ali, J.S. Lange, and S. Stone, Exotics: Heavy Pentaquarks and Tetraquarks, Prog. Part. Nucl. Phys. **97**, 123 (2017).
- [7] F.-K. Guo, C. Hanhart, U.-G. Meißner, Q. Wang, Q. Zhao, and B.-S. Zou, Hadronic molecules, Rev. Mod. Phys. **90**, 015004 (2018).
- [8] S.L. Olsen, T. Skwarnicki, and D. Zieminska, Nonstandard heavy mesons and baryons: Experimental evidence, Rev. Mod. Phys. **90**, 015003 (2018).
- [9] N. Brambilla, S. Eidelman, C. Hanhart, A. Nefediev, C.-P. Shen, C.E. Thomas, A. Vairo, and C.-Z. Yuan, The XYZ states: Experimental and theoretical status and perspectives, Phys. Rept. **873**, 1 (2020).
- [10] R. Aaij et al. (LHCb Collaboration), Observation of a Narrow Pentaquark State, $P_c(4312)^+$, and of the Two-Peak Structure of the $P_c(4450)^+$, Phys. Rev. Lett. **122**,

TABLE I. Particle momenta (center-of-mass frame) that hits triangle singularity (TS) of the upper triangle in Fig. 1(a) and being closest to TS of the lower triangle. All momenta in the loops are collinear and $p_{\bar{K}}$ is taken along the positive axis. $E_3 \equiv E_{\bar{K}} + E_{\Sigma_c^{(*)}} + E_{\bar{D}^{(*)}}$. The first column specifies the DT amplitude from Eqs. (23)-(28). The unit of the entries is MeV.

	$p_{\bar{K}}$	$p_{\bar{K}^*}$	p_{π}	$p_{\Lambda_c^+}$	$p_{\bar{D}^{(*)}}$	$p_{\Sigma_c^{(*)}}$	$E_3 - E$
$A_{\Sigma_c \bar{D}}^{\text{DT}}$	1082	1006	-76	-539	-467	-614	23
$A_{\Sigma_c^* \bar{D}}^{\text{DT}}$	1082	1006	-75	-554	-452	-629	-1880
$A_{\Sigma_c \bar{D}^*}^{\text{DT}}$	953	859	-94	-430	-429	-524	16
$A_{\Sigma_c^* \bar{D}^*}^{\text{DT}}$	953	859	-94	-457	-402	-551	-1947

222001 (2019).

- [11] R. Aaij et al. (LHCb Collaboration), Observation of $J/\psi p$ resonances consistent with pentaquark states in $\Lambda_b^0 \rightarrow J/\psi p K^-$ decays, Phys. Rev. Lett. **115**, 072001 (2015).
- [12] P.A. Zyla et al. (Particle Data Group), The Review of Particle Physics, Prog. Theor. Exp. Phys. **2020**, 083C01 (2020).
- [13] M.-Z. Liu, Y.-W. Pan, F.-Z. Peng, M.S. Sánchez, L.-S. Geng, A. Hosaka, and M.P. Valderrama, Emergence of a complete heavy-quark spin symmetry multiplet: seven molecular pentaquarks in light of the latest LHCb analysis, Phys. Rev. Lett. **122**, 242001 (2019).
- [14] C.-W. Xiao, J. Nieves, and E. Oset, Heavy quark spin symmetric molecular states from $\bar{D}^{(*)} \Sigma_c^{(*)}$ and other coupled channels in the light of the recent LHCb pentaquarks, Phys. Rev. D **100**, 014021 (2019).
- [15] C.-J. Xiao, Y. Huang, Y.-B. Dong, L.-S. Geng, and D.-Y. Chen, Exploring the molecular scenario of $P_c(4312)^+$, $P_c(4440)^+$, and $P_c(4457)^+$, Phys. Rev. D **100**, 014022 (2019).
- [16] Z.-H. Guo and J.A. Oller, Anatomy of the newly observed hidden-charm pentaquark states: $P_c(4312)^+$, $P_c(4440)^+$, and $P_c(4457)^+$, Phys. Lett. B **793**, 144 (2019).
- [17] J. He, Study of $P_c(4457)^+$, $P_c(4440)^+$, and $P_c(4312)^+$ in a quasipotential Bethe-Salpeter equation approach, Eur. Phys. J. C **79**, 393 (2019).
- [18] F.-K. Guo, H.-J. Jing, U.-G. Meißner, and S. Sakai, Isospin breaking decays as a diagnosis of the hadronic molecular structure of the $P_c(4457)^+$, Phys. Rev. D **99**, 091501(R) (2019).
- [19] H.-X. Chen, W. Chen, and S.-L. Zhu, Possible interpretations of the $P_c(4312)^+$, $P_c(4440)^+$, and $P_c(4457)^+$, Phys. Rev. D **100**, 051501(R) (2019).
- [20] R. Chen, Z.-F. Sun, X. Liu, and S.-L. Zhu, Strong LHCb evidence supporting the existence of the hidden-charm molecular pentaquarks, Phys. Rev. D **100**, 011502(R) (2019).
- [21] G.-J. Wang, L.-Y. Xiao, R. Chen, X.-H. Liu, X. Liu, and S.-L. Zhu, Probing hidden-charm decay properties of P_c states in a molecular scenario, Phys. Rev. D **102**, 036012 (2020).
- [22] T. Gutsche and V.E. Lyubovitskij, Structure and decays of hidden heavy pentaquarks, Phys. Rev. D **100**, 094031 (2019).
- [23] B. Wang, L. Meng, and S.-L. Zhu, Hidden-charm and hidden-bottom molecular pentaquarks in chiral effective field theory, JHEP **11**, 108 (2019).
- [24] J. He and D.-Y. Chen, Molecular states from $\Sigma_c^{(*)} \bar{D}^{(*)}$ -

TABLE II. Particle momenta that hits TS of the lower triangle in Fig. 1(a) and being closest to TS of the upper triangle. $E_1 \equiv E_{\bar{K}^*} + E_{\Lambda_c} + E_{\bar{D}^{(*)}}$. The other features are the same as Table I.

	$p_{\bar{K}}$	$p_{\bar{K}^*}$	p_{π}	$p_{\Lambda_c^+}$	$p_{\bar{D}^{(*)}}$	$p_{\Sigma_c^{(*)}}$	$E_1 - E$
$A_{\Sigma_c \bar{D}}^{\text{DT}}$	1061	926	-135	-471	-455	-607	-76
$A_{\Sigma_c^* \bar{D}}^{\text{DT}}$	1006	771	-234	-346	-426	-580	-211
$A_{\Sigma_c \bar{D}^*}^{\text{DT}}$	937	807	-131	-412	-395	-543	-45
$A_{\Sigma_c^* \bar{D}^*}^{\text{DT}}$	879	654	-225	-266	-388	-491	-164

- $\Lambda_c \bar{D}^{(*)}$ interaction, Eur. Phys. J. C **79**, 887 (2019).
- [25] Y.-H. Lin and B.-S. Zou, Strong decays of the latest LHCb pentaquark candidates in hadronic molecule pictures, Phys. Rev. D **100**, 056005 (2019).
- [26] T.J. Burns and E.S. Swanson, Molecular interpretation of the $P_c(4440)^+$ and $P_c(4457)^+$ states, Phys. Rev. D **100**, 114033 (2019).
- [27] Y.-J. Xu, C.-Y. Cui, Y.-L. Liu, and M.-Q. Huang, Partial decay widths of $P_c(4312)$ as a $\bar{D}\Sigma_c$ molecular state, Phys. Rev. D **102**, 034028 (2020).
- [28] Y. Yamaguchi, H. García-Tecocoatzí, A. Giachino, A. Hosaka, and E. Santopinto, P_c pentaquarks with chiral tensor and quark dynamics, Phys. Rev. D **101**, 091502(R) (2020).
- [29] S. Sakai, H.-J. Jing, and F.-K. Guo, Decays of P_c into $J/\psi N$ and $\eta_c N$ with heavy quark spin symmetry, Phys. Rev. D **100**, 074007 (2019).
- [30] M.B. Voloshin, Some decay properties of hidden-charm pentaquarks as baryon-meson molecules, Phys. Rev. D **100**, 034020 (2019).
- [31] Q. Wu and D.-Y. Chen, Production of P_c states from Λ_b decay, Phys. Rev. D **100**, 114002 (2019).
- [32] J.-R. Zhang, Exploring a $\Sigma_c \bar{D}$ state: with focus on $P_c(4312)^+$, Eur. Phys. J. C **79**, 1001 (2019).
- [33] H. Xu, Q. Li, C.-H. Chang, and G.-L. Wang, Recently observed P_c as molecular states and possible mixture of $P_c(4457)$, Phys. Rev. D **101**, 054037 (2020).
- [34] M.-L. Du, V. Baru, F.-K. Guo, C. Hanhart, U.-G. Meißner, J.A. Oller, and Q. Wang, Interpretation of the LHCb P_c states as hadronic molecules and hints of a narrow $P_c(4380)$, Phys. Rev. Lett. **124**, 072001 (2020).
- [35] M.-L. Du, V. Baru, F.-K. Guo, C. Hanhart, U.-G. Meißner, J.A. Oller, and Q. Wang, Revisiting the nature of the P_c pentaquarks, arXiv:2102.07159 [hep-ph].
- [36] C.-W. Xiao, J.-X. Lu, J.-J. Wu, and L.-S. Geng, How to reveal the nature of three or more pentaquark states, Phys. Rev. D **102**, 056018 (2020).
- [37] A. Ali and A.Ya. Parkhomenko, Interpretation of the narrow $J/\psi p$ peaks in $\Lambda_b \rightarrow J/\psi p K^-$ decay in the compact diquark model, Phys. Lett. B **793**, 365 (2019).
- [38] A. Pimikov, H.-J. Lee, and P. Zhang, Hidden charm pentaquarks with color-octet substructure in QCD Sum Rules, Phys. Rev. D **101**, 014002 (2020).
- [39] Z.-G. Wang, Analysis of the $P_c(4312)$, $P_c(4440)$, $P_c(4457)$ and related hidden-charm pentaquark states with QCD sum rules, Int. J. Mod. Phys. A **35**, 2050003 (2020).
- [40] R. Zhu, X. Liu, H. Huang, and C.-F. Qiao, Analyzing doubly heavy tetra- and penta-quark states by variational method, Phys. Lett. B **797**, 134869 (2019).
- [41] X.-Z. Weng, X.-L. Chen, W.-Z. Deng, and S.-L. Zhu, Hidden-charm pentaquarks and P_c states, Phys. Rev. D **100**, 016014 (2019).
- [42] F. Giannuzzi, Heavy pentaquark spectroscopy in the diquark model, Phys. Rev. D **99**, 094006 (2019).
- [43] F. Stancu, Spectrum of the $uudc\bar{c}$ hidden charm pentaquark with an $SU(4)$ flavor-spin hyperfine interaction, Eur. Phys. J. C **79**, 957 (2019).
- [44] Y. Dong, P. Shen, F. Huang, and Z. Zhang, Selected strong decays of pentaquark State $P_c(4312)$ in a chiral constituent quark model, Eur. Phys. J. C **80**, 341 (2020).
- [45] M.I. Eides, V.Yu Petrov, and M.V. Polyakov, New LHCb pentaquarks as hadrocharmonium states, Mod. Phys. Lett. A **35**, 2050151 (2020).
- [46] C. Fernández-Ramírez, A. Pilloni, M. Albaladejo, A. Jackura, V. Mathieu, M. Mikhasenko, J.A. Silva-Castro, and A.P. Szczepaniak, Interpretation of the LHCb $P_c(4312)^+$ Signal, Phys. Rev. Lett. **123**, 092001 (2019).
- [47] S.-Q. Kuang, L.-Y. Dai, X.-W. Kang, and D.-L. Yao, Pole analysis on the hadron spectroscopy of $\Lambda_b^0 \rightarrow J/\psi p K^-$, Eur. Phys. J. C **80**, 433 (2020).
- [48] Q. Wang, X.-H. Liu, and Q. Zhao, Photoproduction of hidden charm pentaquark states $P_c^+(4380)$ and $P_c^+(4450)$, Phys. Rev. D **92**, 034022 (2015).
- [49] V. Kubarovsky and M.B. Voloshin, Formation of hidden-charm penta quarks in photon-nucleon collisions, Phys. Rev. D **92**, 031502(R) (2015).
- [50] M. Karliner and J.L. Rosner, Photoproduction of Exotic Baryon Resonances, Phys. Lett. B **752**, 329 (2016).
- [51] Studying the $P_c(4450)$ resonance in J/ψ photoproduction off protons, A.N. Hiller Blin, C. Fernández-Ramírez, A. Jackura, V. Mathieu, V.I. Mokeev, A. Pilloni, and A.P. Szczepaniak, Phys. Rev. D **94**, 034002 (2016).
- [52] X.-Y. Wang, X.-R. Chen, and J. He, Possibility to study pentaquark states $P_c(4312)$, $P_c(4440)$, and $P_c(4457)$ in $\gamma p \rightarrow J/\psi p$ reaction, Phys. Rev. D **99**, 114007 (2019).
- [53] J.-J. Wu, T.-S.H. Lee, and B.-S. Zou, Nucleon resonances with hidden charm in γp reactions, Phys. Rev. C **100**, 035206 (2019).
- [54] X. Cao and J.-P. Dai, Confronting pentaquark photoproduction with new LHCb observations, Phys. Rev. D **100**, 054033 (2019).
- [55] A. Ali et al. (GlueX Collaboration), First measurement of near-threshold J/ψ exclusive photoproduction off the proton, Phys. Rev. Lett. **123**, 072001 (2019).
- [56] F.-K. Guo, X.-H. Liu, and S. Sakai, Threshold cusps and triangle singularities in hadronic reactions, Prog. Part. Nucl. Phys. **112**, 103757 (2020).
- [57] R. Aaij et al. (LHCb Collaboration), Evidence for exotic hadron contributions to $\Lambda_b^0 \rightarrow J/\psi p \pi^-$ decays, Phys. Rev. Lett. **117**, 082003 (2016).
- [58] S.X. Nakamura, Triangle singularity appearing as an $X(3872)$ -like peak in $B \rightarrow (J/\psi \pi^+ \pi^-) K \pi$, Phys. Rev. D **102**, 074004 (2020).
- [59] U. Skerbis and S. Prelovsek, Nucleon- J/ψ and nucleon- η_c scattering in P_c pentaquark channels from LQCD, Phys. Rev. D **99**, 094505 (2019).
- [60] S.X. Nakamura, Coupled-channel analysis of $D^+ \rightarrow K^- \pi^+ \pi^+$ decay, Phys. Rev. D **93**, 014005 (2016).
- [61] X.-K. Dong, F.-K. Guo, and B.-S. Zou, Why there are many threshold structures in hadron spectrum with heavy quarks, arXiv:2011.14517 [hep-ph].
- [62] H. Kamano, S.X. Nakamura, T.-S.H. Lee, and T. Sato, Unitary coupled-channels model for three-mesons decays of heavy mesons, Phys. Rev. D **84**, 114019 (2011).